Journal of Engineering Research and Applied Science
Available at www.journaleras.com
Volume 8 (2), December 2019, pp 1216-1228
ISSN 2147-3471 © 2019

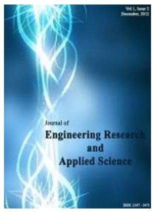

Petrology of the paleozoic plutons in Eastern pontides: artabel pluton (Gümüşhane, NE Turkey)

A.Vural[1,a], A.Kaygusuz[1]

Gümüşhane University, Department of Geological Engineering, Gümüşhane, Turkey

Accepted 12 September 2019

Abstract
There are many Paleozoic to Tertiary plutons in Eastern Pontides with different compositions, sizes and age intervals. Of these plutons, especially the Paleozoic aged plutons are frequently observed in the southern part of Eastern Pontides, whereas they are rarely located in the northern part. In this study, the petrographic and geochemical characteristics of the Paleozoic Artabel Pluton are presented in order to explain the origin and evolutionary processes of the rocks. Artabel Pluton is granite in composition with primary minerals including plagioclase, quartz, orthoclase, biotite, muscovite and Fe-Ti oxide. The rocks of the pluton have medium to high-K calc-alkaline characters with I-type features. They are enriched by light rare earth elements (LREE) and large ion lithophile elements (LILE) with pronounced depleted by high field strength elements (HFSE). The $La_{(n)}/Lu_{(n)}$ ratios of the rocks vary between 4.9 and 8.9, and they display negative Eu anomalies (Eu/Eu*=0.3-0.6). Major and trace element variations indicate that plagioclase and Fe-Ti oxide fractionation is effective in the development of the rocks. Crystallization temperatures calculated according to apatite-zirconium geothermometer range between 690 and 897 °C. All these characteristics, high SiO_2, moderate (Al_2O_3) / $(FeO+MgO+TiO_2)$, (Na_2O+K_2O) / $(FeO_T+MgO+TiO_2)$ and low (CaO) / $(FeO_T+MgO+TiO_2)$ content indicate that the rocks of the Artabel Pluton may have been formed by the partial melting of meta-magmatic source rocks.

Keywords: paleozoic, artabel pluton, geochemistry, petrology, Gümüşhane, Eastern Pontides.

1. Introduction

Volcanic and plutonic rocks are frequently observed in the Eastern Pontides located on the Alpine-Himalaya orogenic belt. There are many of the plutons in the region with a wide range of composition and age interval from the Permo-Carboniferous to Eocene-Oligocene (Figure 1). These granitic plutons are settled in three different time periods as Paleozoic, Cretaceous and Eocene (Figure 1). Of these, the Paleozoic plutons [1-5] have settled by cutting through the metamorphic rocks. These plutons are found in the Southern Zone (Gümüşhane, Köse and Artvin) as large blocks [1-2] and as smaller blocks in the Northern Zone (Trabzon-Maçka-Özdil-Tonya) [4-5]. Moreover, Early Jurassic Plutons have settled by cutting through the metamorphic basement rocks [3, 6-7] (Figure 1). Late Cretaceous plutons are cut the volcanic and/or volcanoclastic rocks related to subduction [8-11]. Whereas Eocene and post-Eocene plutons have settled in narrower regions cutting through all units [8, 12-17] (Figure 1).

Even though there are many studies on the ore geology, general geology and petrology of the magmatic rocks in the region [18-27], no studies have been carried out on the Artabel Pluton excluding those by [28]. The aim of the present study was to present petrographic and geochemical characteristics of the Artabel Pluton for clarifying the development of the Paleozoic magmatism in the eastern Pontides.

2. Regional geology and geological setting

The basement of the Eastern Pontides is made up the Early Carboniferous metamorphic rocks and Late Carboniferous plutonic rocks [2, 4, 5, 29-31]. These basement rocks are uncomfortably overlain by Early-Middle Jurassic volcano-sedimentary sequence [32-33]. Early-Late Jurassic granitic plutons [7, 34] have cut through these units. Late Jurassic-Cretaceous period is characterized by extensive carbonate deposits in the Eastern Pontides. Late Cretaceous granitic plutons and volcanic rocks comprise the dominant lithology in the northern zone [8, 9, 15, 27, 35], while sedimentary rocks

[a]Corresponding author; abdullah.kaygusuz@gmail.com

have been dominant in the southern zone during this period. Anatolid-Tauride blocks have collided during the Late Paleocene-Early Eocene period [36]. Formation of the adakitic and non-adakitic rocks during the Early Eocene [37-41] is considered as the final stage of the arc-continent collision. Eocene period in the region is represented by post-collision calc-alkaline volcanic rocks and high-K calc-alkaline and shoshonitic plutons [10, 13, 25, 37, 41-45]. Post-Eocene uplift and erosion brought clastic input into locally developed basins [46]. In the Late Eocene, the region has remained largely above sea level with continuous minor volcanism and terrigenous sedimentation [36]. The Miocene and post-Miocene magmatism are characterized by calc-alkaline to mildly alkaline compositions [40, 47-48], while the Miocene to Pliocene volcanism in the Ilıca-Kandilli area is represented by calc-alkaline in compositions [49-50]. The youngest rocks in the region are comprised of Quaternary travertines and alluviums.

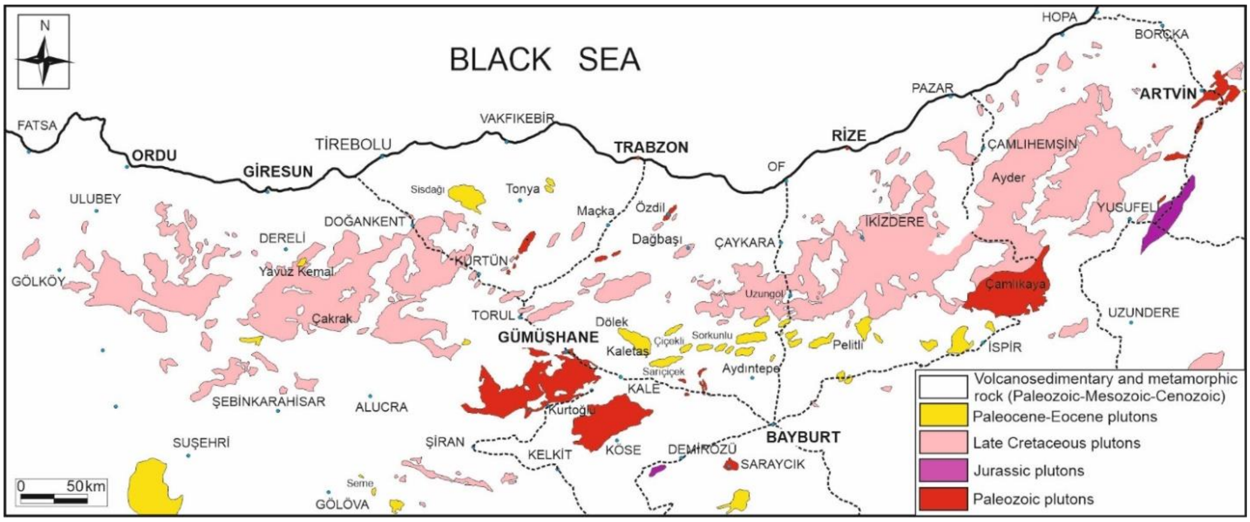

Figure 1. Geological map showing the plutonic and surrounding rocks in the Eastern Pontides (modified from [17]).

The study area is located to the south of the Eastern Pontides. Permo-Carboniferous granites make up the oldest units in the study area (Figure 2). These basement rocks are overlaid by Early-Middle Jurassic volcano-sedimentary rocks (Zimonköy Formation) with unconformity. Late Jurassic-Early Cretaceous Berdiga Formation conformably overlay these units. Late Cretaceous rocks are represented by the Kermutdere Formation starting at the basement with sandy limestones, continue with red limestones, and ending with volcano-sedimentary series. Eocene Alibaba Formation uncomfortably overlays the Cretaceous units consisting of sedimentary interfingered by andesite, basalt and their pyroclastic. All these units are cut through by Lutetian (44 Ma) Avliyana Granitoid (Figure 2). The youngest units of the study area are made up of Quaternary alluviums and travertines.

3. Analysis methods

The scope of this study, thin sections were prepared from 50 rock samples obtained in the field and detailed petrographic characteristics were determined with a polarizing microscope and modal analyses of 10 samples were performed.

Major, trace and rare earth element analyses for the 9 samples of the Artabel Pluton were carried out at the ACME Analytical Laboratory (Vancouver, Canada). The 0.2 gr powder rock sample prepared for main and trace element analyses was first dissolved with 1.5 gr $LiBO_2$ and with 100 ml %5 HNO_3 afterwards followed by measurements via induction coupled plasma atomic emission spectrometer (ICP-AES). Rare earth elements (REEs) were analyzed via induction coupled plasma mass spectrometer (ICP-MS) after the 0.25 gr powder rock sample was dissolved in four different acids. Loss on ignition was calculated from the weight difference after the samples were burned at 1000 ^{o}C.

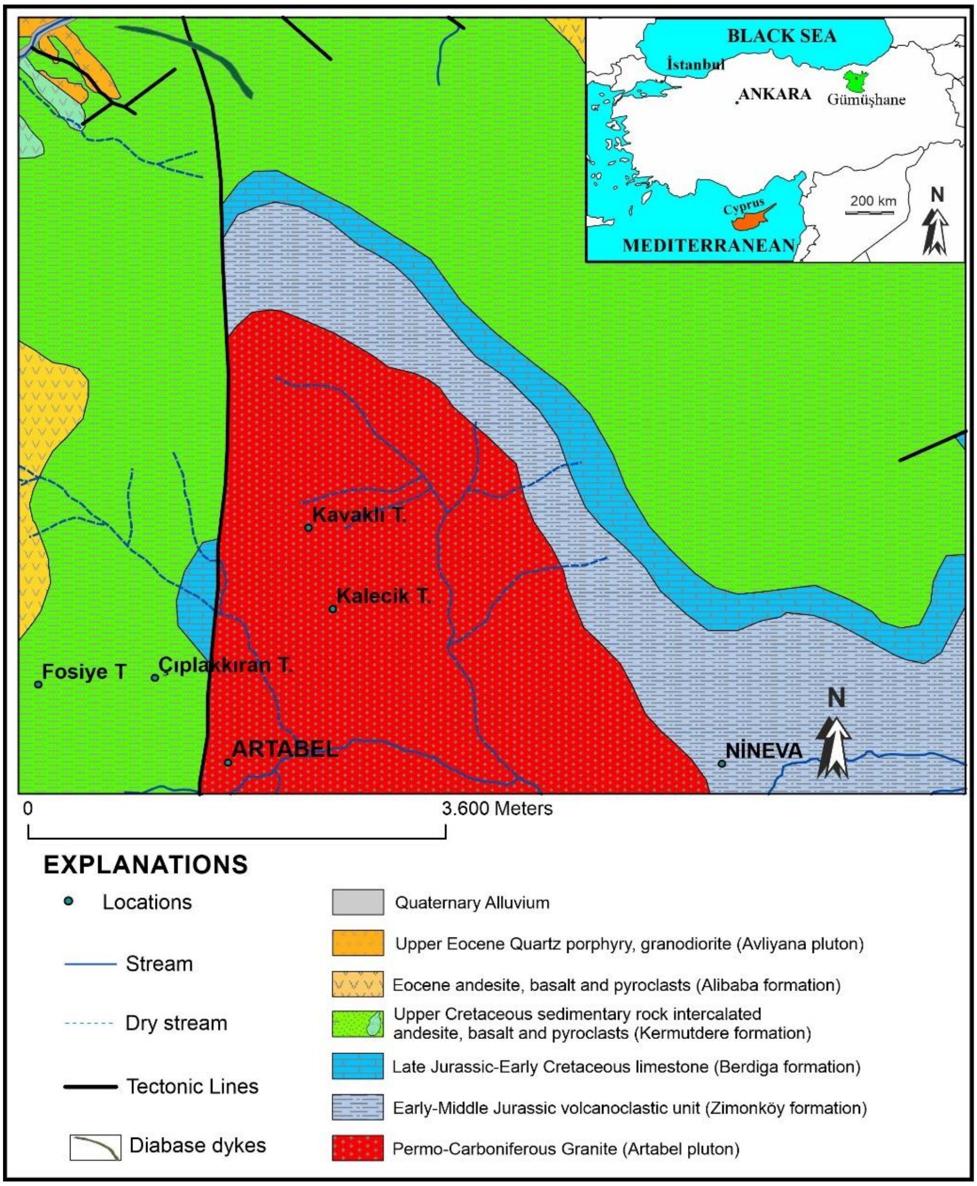

Figure 2. Geology map of the study area and its surroundings (modified from [28]).

4. Results

4.1. Field observations

The rocks of the Artabel Pluton outcrops over an area of 12 km² (Figure 2). They are observed in the Artabel, Çıplakkıran Hill, Kayaklı Hill and Nineva to the south-southeast of the study area. Tectonic relations with the surrounding rocks are observed especially at the Artabel village and Çıplakkıran Hill. The large tectonic line observed in the N-S direction at this area has a length of about 8 km up to the Avliyana village. Structures with multiple cracks and fractures have developed at some areas and the blocks of the rocks are not effective. The formations of the arena are observed especially near and to the east of the Artabel village. Macroscopically large orthoclase, quartz and less plagioclase minerals can be detected.

4.2. Petrographic features

The petrographic characteristics and modal analysis results of the Artabel Pluton have been presented in detail by [28]. Rock samples of the Artabel Pluton have granite composition in the QAP diagram based on modal analysis [28, 51]. The rocks of the pluton display granular, poikilitic and micrographic texture. Primary minerals are plagioclase (% 31-36), quartz (% 28-35), orthoclase (% 27-31), biotite (% 1-4), muscovite (% 0.2-0.5) and opaque minerals (% 1-3) (Figure 3).

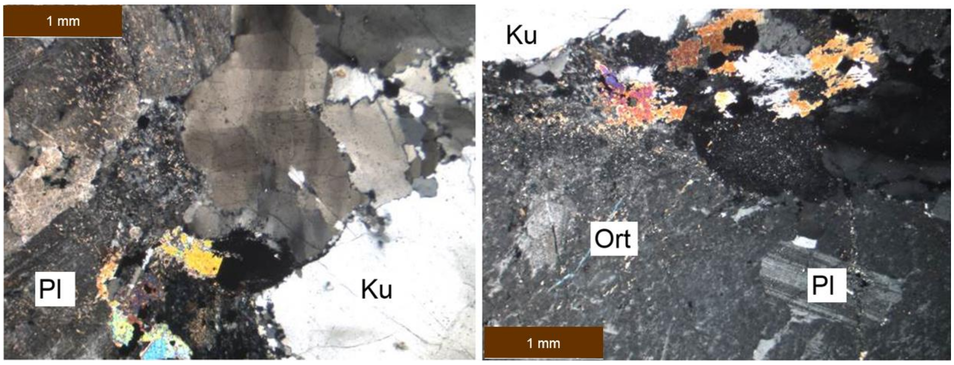

Figure 3. Microscopic images showing the rocks of the Artabel Pluton, a) Medium to large granular texture observed in the granites, b) Large orthoclase minerals include small plagioclase crystals (Pl: Plagioclase, Ku: Quartz, Ort: Orthoclase).

5. Geochemical characteristics

The SiO_2 values of the rock samples vary in a narrow interval (75-77 %). The CaO, Fe_2O_{3T}, K_2O, Al_2O_3 contents of the rocks vary between 0.3-1.2, 1.1-1.8, 2.8-4.9 and 13-14, respectively. While the K_2O/Na_2O ratios of the samples vary between 0.7-2.3, A/CNK (molar $Al_2O_3/CaO+Na_2O+K_2O$) values vary between 1.1-1.7 and magnesium numbers [100 x (MgO/MgO + Fe_2O_{3T})] vary between 24 and 49 (Table 1).

Plotted on the SiO_2 vs. (Na_2O+K_2O) diagram, the samples are granite in composition and has sub-alkaline characters (Figure 4a). Samples in the Artabel Pluton have medium to high-K content in the K_2O vs. SiO_2 diagram (Figure 4b).

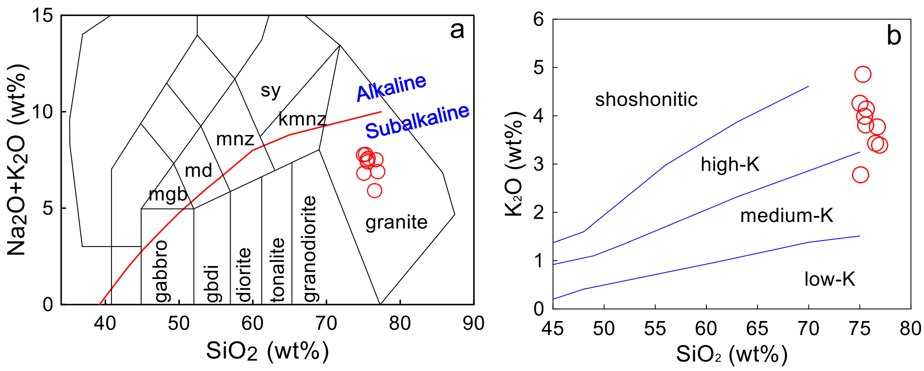

Figure 4. (a) (Na_2O+K_2O) vs. SiO_2 classification diagram [52], (b) K_2O vs. SiO_2 diagram [53] for the samples of the Artabel Pluton.

While a negative correlation is observed between TiO_2, P_2O_5, Al_2O_3, $Fe_2O_3^T$, CaO and Na_2O vs. SiO_2 variation diagrams (Figure 5), a positive relationship is observed between SiO_2 and K_2O.

Table 1 presents the whole-rock major, trace and rare earth element analysis results for the 9 samples of the Artabel Pluton.

Rock type	**granite**								
Sample no	GT-8	AVL-9	GT-7	GT-28	GT-14	GT-10	GT-16	GT-12	GT-9
SiO_2	75.02	75.07	75.30	75.48	75.57	75.64	76.54	76.71	76.95
TiO_2	0.08	0.18	0.09	0.09	0.09	0.07	0.02	0.09	0.09
Al_2O_3	13.21	14.00	14.05	13.30	13.23	13.11	12.72	12.90	12.72
Fe_2O_3	1.77	1.09	1.11	1.22	1.43	1.05	1.35	1.23	1.30
MnO	0.03	0.02	0.01	0.02	0.02	0.02	0.03	0.02	0.01
MgO	0.28	0.17	0.33	0.43	0.25	0.45	0.51	0.32	0.19
CaO	0.65	1.22	0.43	0.68	0.66	0.87	0.78	0.55	0.29
Na_2O	3.51	4.03	2.93	3.50	3.59	3.44	2.48	3.74	3.50
K_2O	4.26	2.78	4.86	3.99	3.81	4.14	3.43	3.77	3.39
P_2O_5	0.03	0.04	0.02	0.04	0.04	0.03	0.02	0.03	0.02
LOI	1.00	1.30	0.70	1.20	1.20	1.10	2.00	0.50	1.40
Total	99.84	99.90	99.83	99.95	99.89	99.92	99.88	99.86	99.86
Co	0.50	1.10	0.90	0.30	0.30	0.40	0.60	0.80	0.20
Ni	3.90	1.50	3.10	2.80	2.40	2.50	3.10	3.60	2.50
V	8.00	14.00	11.00	8.00	8.00	8.00	8.00	8.00	8.00
Cu	4.70	5.50	4.70	2.80	3.60	2.80	4.60	6.60	4.50
Pb	3.90	11.90	4.60	4.40	4.90	4.70	4.60	3.90	4.70
Zn	16.00	13.00	6.00	13.00	14.00	9.00	16.00	8.00	4.00
W	0.50	0.50	1.80	1.00	3.90	0.50	0.90	0.50	1.30
Rb	136.90	26.30	124.50	123.40	119.10	106.50	111.30	115.40	87.90
Ba	730.00	332.00	726.00	500.00	561.00	641.00	369.00	589.00	617.00
Sr	76.50	173.00	71.60	84.90	67.20	83.30	65.40	85.30	55.40
Ta	1.00	0.80	1.00	0.80	1.10	0.70	0.90	0.90	0.80
Nb	7.90	8.70	8.00	7.40	8.70	7.50	5.60	8.70	8.80
Hf	2.70	3.30	3.20	2.90	3.30	2.60	2.30	2.90	2.90
Zr	83.10	106.20	96.70	82.90	95.90	76.60	58.60	88.70	99.50
Ti	477.30	1073.92	536.96	536.96	536.96	417.63	119.32	536.96	536.96
Y	22.50	24.40	23.70	23.40	27.00	24.60	29.80	20.50	26.60
Th	12.10	14.50	14.80	12.90	14.10	12.70	13.80	12.30	11.20
U	4.00	2.90	3.00	3.70	3.10	2.10	4.80	2.90	1.90
Ga	14.90	13.10	14.60	14.00	16.20	15.10	14.20	14.50	14.40
La	25.70	34.30	29.30	24.40	25.20	23.20	19.40	24.50	30.70
Ce	49.00	60.80	54.20	49.20	49.70	45.50	43.40	46.20	55.60
Pr	5.18	6.00	5.78	4.83	5.10	4.69	4.84	4.86	5.99
Nd	17.70	20.80	19.60	17.70	18.40	15.90	18.70	17.30	23.10
Sm	3.65	3.12	4.10	3.29	3.66	3.66	4.10	3.32	4.19
Eu	0.48	0.67	0.52	0.48	0.46	0.53	0.42	0.44	0.45
Gd	3.61	3.37	4.25	3.16	3.99	3.55	4.15	3.20	3.99
Tb	0.60	0.57	0.72	0.57	0.63	0.64	0.72	0.54	0.68
Dy	3.76	3.38	4.05	3.49	4.11	3.79	4.44	3.07	4.20
Ho	0.80	0.74	0.81	0.78	0.90	0.80	0.90	0.62	0.95
Er	2.45	2.46	2.45	2.34	2.78	2.48	2.80	2.10	2.40
Tm	0.35	0.37	0.37	0.36	0.43	0.36	0.41	0.32	0.43
Yb	2.78	2.40	2.56	2.57	2.90	2.52	2.72	2.06	2.93
Lu	0.39	0.40	0.37	0.38	0.45	0.38	0.41	0.32	0.45
(Eu/Eu*)n	0.40	0.63	0.38	0.45	0.37	0.44	0.31	0.41	0.33
(La/Lu)n	6.82	8.88	8.20	6.65	5.80	6.32	4.90	7.93	7.06
Mg #	25.83	25.56	39.56	43.69	27.79	48.55	45.41	36.42	24.34
A /CNK (ASI)	1.14	1.18	1.29	1.18	1.18	1.12	1.57	1.15	1.28
K_2O/Na_2O	1.21	0.69	1.66	1.14	1.06	1.20	2.32	1.01	0.97
T °C (zircon)	747	770	769	749	762	739	736	754	773
T °C (apatite)	843	868	813	871	872	849	824	858	828

Mg#=100xMgO/(MgO+Fe_2O_{3T}), A/CNK=Mol Al_2O_3/(CaO+Na_2O+K_2O), Fe_2O_3: Total iron, Eu*=$(Sm+Gd)_N$ /2

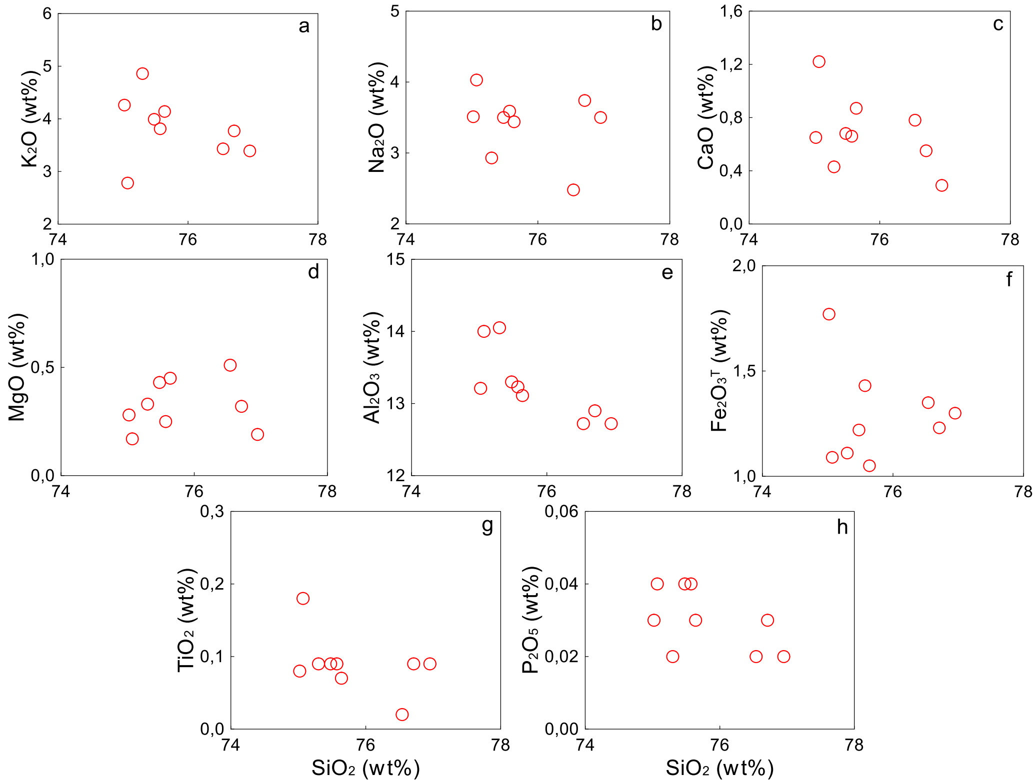

Figure 5. SiO_2 (wt.%) vs. major oxides (wt.%) for rock samples from the studied pluton.

While Rb, Zr, Ba, Y and Pb display a positive correlation with increasing a SiO_2, a negative correlation is observed for Th, Nb, Sr and Ni (Figure 6). These correlations observed in the rocks indicate that fractional crystallization has played an important role in the formation of these rocks.

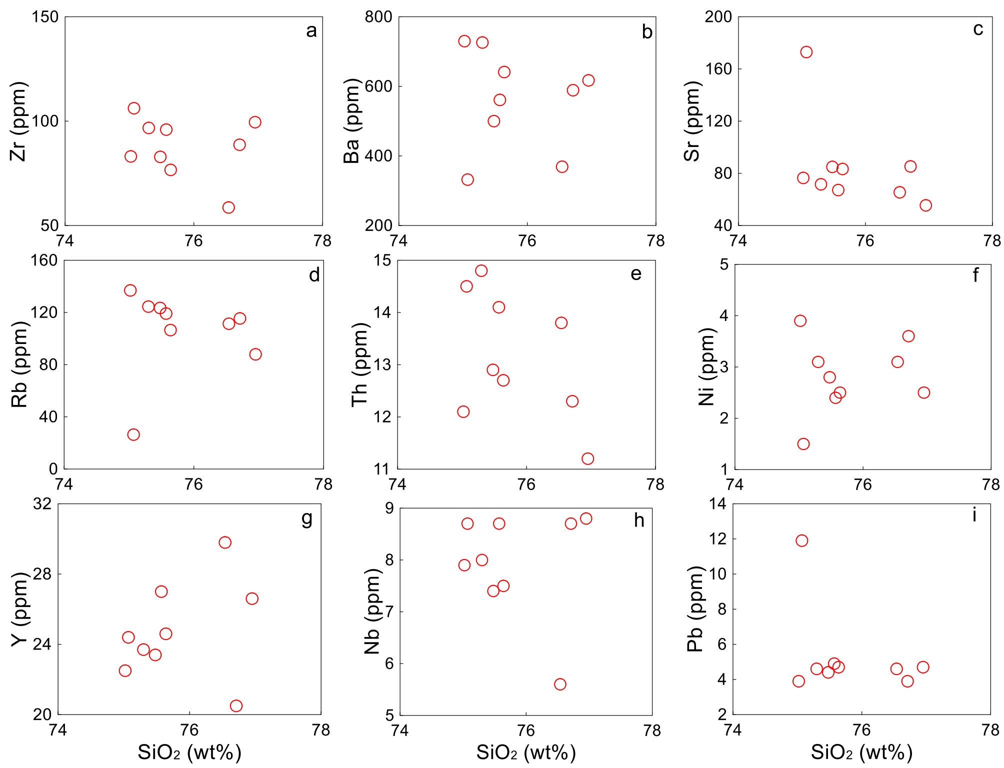

Figure 6. SiO_2 (wt.%) vs. trace elements (ppm) for rock samples from the studied pluton.

In primitive mantle-normalized [54] multi-element variation diagrams (Figure 7a), all of the rock samples show enrichments in the large-ion lithophile elements (LILEs; Rb, Ba, Th, U) and depletions in the high-field strength elements (HFSEs; Nb, P and Ti). In chondrite-normalized REE [55] diagrams, the samples from the plutons (Figure 7b) show enrichment in light REE and relatively flat heavy REE distribution. The $(La/Lu)_N$ values of the samples vary between 4.9-8.9 and they display negative Eu anomalies ($Eu/ Eu^*_{(n)}$ = 0.3-0.6) (Figure 7b).

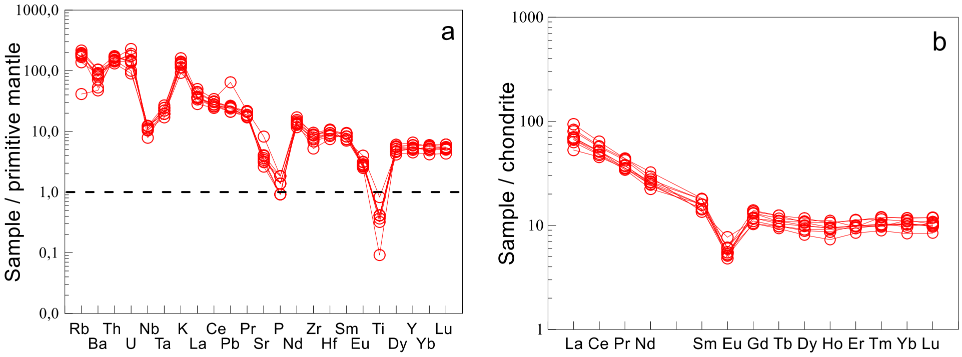

Figure 7. Trace element variations of the Artabel Pluton, a) Primitive mantle-normalized [54] trace element patterns, b) Chondrite-normalized [55] rare earth element patterns.

6. Geothermometer

Apatite and zircon saturation temperatures [56-58] are calculated based on the whole-rock geochemical analyses of the rock samples correspond to the minimum or maximum temperature limits for the intruding magma, depending on whether the melt was saturated or undersaturated with these components. The crystallization temperatures of the rock changes from 838 to 842 ºC based on the calculations using the zircon values, and from 739 to 872 ºC based on the calculations using the apatite values (Table 1).

7. Tectonic setting

All samples plot in the I-type granitoid area on Nb vs. 10000Ga/Al diagram [59] (Figure 8a). Negative P_2O_5 correlation increasing SiO_2 supports I-type trend (Figure 5). In the K_2O vs. Na_2O diagram (Figure 8b), majority of the samples plot on the Lachlan Fold Belt [60].

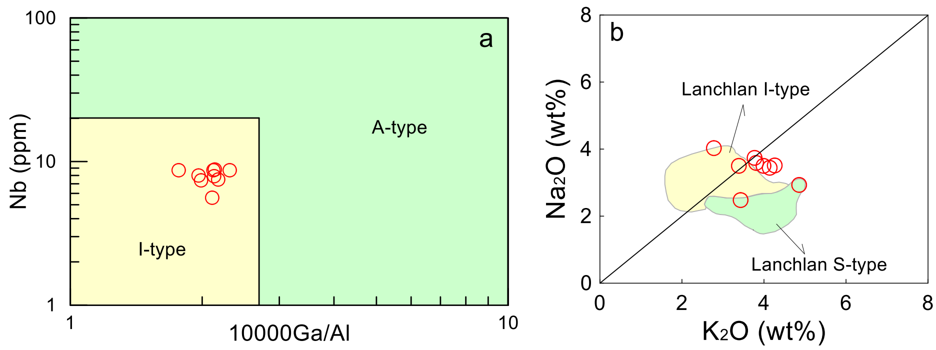

Figure 8. (a) Nb vs. 10000Ga/Al [59] diagram, (b) Na_2O vs. K_2O diagram. I and S-type areas from [60].

The samples from the pluton plot in the volcanic arc field in the Sr/Y vs. Y diagram [61] (Figure 9a). Applying the discrimination criteria of [62], all samples plot in the fields of volcanic arc granites (VAG) and syn-collisional granites (Syn-COLG) in the Nb vs. Y diagram (Figure 9b), whereas the samples plot in the Post-COLG field in the Rb vs. (Y+Nb) diagram (Figure 9c).

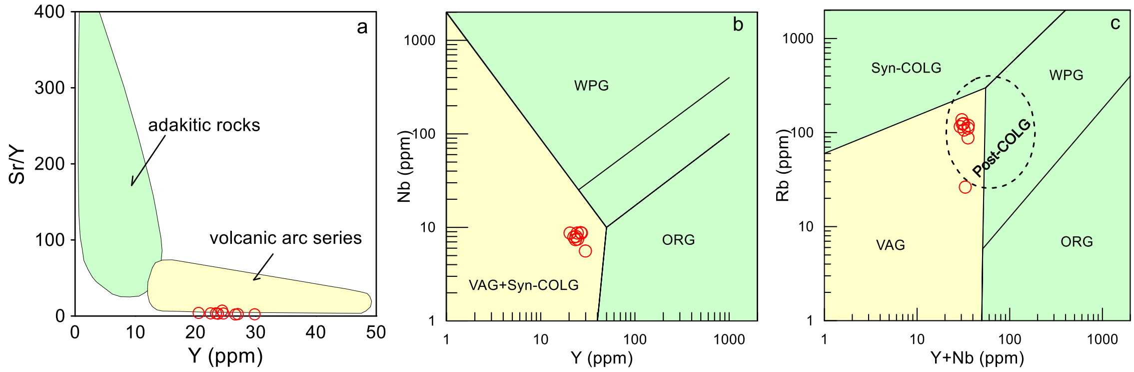

Figure 9. (a) Sr/Y vs. Y [61], (b) Nb vs. Y and (c) Rb vs. (Y+Nb) [62] diagrams.

8. Discussion

8.1. Fractional crystallization (FC)

Most major oxides and trace elements display well-defined positive or negative correlations with increasing SiO_2 content (Figure 5) indicate that fractional crystallization has played an important role in the development of these rocks. In Harker diagrams (Figures 5 and 6), increasing SiO_2 with decreasing Al_2O_3, TiO_2, CaO, MgO, $Fe_2O_3^T$, P_2O_5, Sr and Ni, and increase K_2O and Rb indicated plagioclase, hornblende, pyroxene, apatite and titanite fractionation. Increasing SiO_2 with K_2O and Rb indicate that K-feldspar and biotite do not play a significant role at fractionation. Negative Ti and Nb anomaly are related to the fractionation of Ti-containing phases; whereas negative P anomaly is related to apatite fractionation. The fractionation of feldspar will also result in the depletion of Ba and Sr. The negative Eu anomalies (Figure 7) and a decrease in Sr with increasing silica (Figure 6) indicate that plagioclase is an important fractionating phase.

The positive correlation between SiO_2 and Y/Nb contents may be related to crustal assimilation. The studied rocks also characterized by pronounced negative Nb-Ta and positive Pb anomalies indicating a subduction signature and/or some crustal contribution.

Two main petrogenetic models are proposed for the origins of felsic magmas: (1) they are derived from basaltic parent magmas by fractional crystallization (FC) or assimilation and fractional crystallization (AFC) processes [63-64]; or (2) considering the principle that mantle-derived basaltic magmas provide heat for the partial melting of crustal rocks [65-66], the felsic magmas are derived by partial melting of meta-igneous [67] or meta-sedimentary rocks [68]. The first model is invalid for the origin of the studied rocks. Because there is no basic composition in any of the geochemical data for the rocks (SiO_2 = % 75-77, Mg# = 24-49, Ni = 2-4). Such voluminous felsic magmas cannot be generated by differentiation of mantle-derived mafic magmas. In addition, rock components do not vary from gabbro to granodiorite or to leucogranite. Moreover, no mafic enclaves were observed in the rocks. All these characteristics indicate that the rocks of the pluton have not originated from a basic magma via AFC. Pluton representing mixtures of basaltic and granitic magmas is also unlikely because coeval basaltic members are lacking in the study area. The

8.2. Magma origin

samples in the Figure 5 and 6 present almost linear trends, and their bulk-rock composition can be related to partial melting. Therefore, a crustal origin of magmas can be considered for the Artabel Pluton.

The differences in the magma composition may be due to the partial melting of different source rocks such as amphibolites, tonalitic gneiss, metagreywacke and metapelite under variable melting conditions and this may be explained by molar oxide ratios or major oxide ratios such as (CaO) / (FeO_T+MgO+TiO_2), (Al_2O_3) / (FeO+MgO+TiO_2) and (Na_2O+K_2O) / (FeO_T+MgO+TiO_2) (Figure 10). Low (CaO) / (FeO_T+MgO+TiO_2) ratios, moderate (Al_2O_3) / (FeO+MgO+TiO_2), (Na_2O+K_2O) / (FeO_T+MgO+TiO_2) values and high SiO_2 contents observed in the studied rocks (Figure 10) indicate that the origin of the rocks may be meta-magmatic rocks.

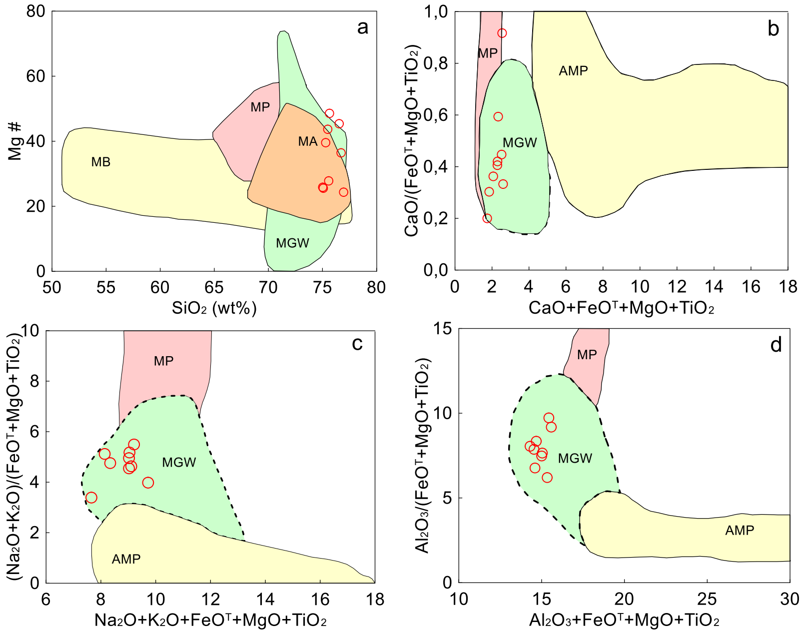

Figure 10. (a-c) Chemical composition for rock samples of the studied pluton. MA: meta-andesites, MB: meta-basalts, MP: metapelites, MGW: metagreywackes, AMP: amphibolites. Sources: [69].

The rock samples of the Artabel Pluton located on the lithospheric mantle area in the La/Yb vs. Nb/La diagram (Figure 11a). The Th/U values of the samples are between 1 and 6, and they are located on the lower-middle continental crust area in the U against Th/U diagram (Figure 11b). Average Nb/Ta ratio is 17.5 for the mantle origin magma and between 11 and 12 for crustal origin magma. The Nb/Ta ratios of the studied samples vary between 6 and 11 (Table 1) indicating crustal origin magmas.

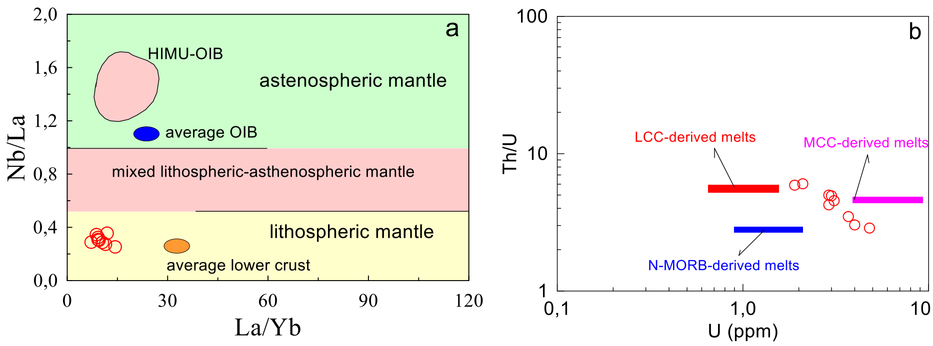

Figure 11. (a) La/Yb vs. Nb/La, (b) U vs. Th/U diagrams for the studied samples.

9. Conclusions

1. Artabel Pluton consists of granite in composition and contains plagioclase, quartz, orthoclase, biotite, muscovite and Fe-Ti oxide minerals.
2. Artabel Pluton has peraluminous, medium-to-high-K calc-alkaline, and I-type features.
3. Main and trace element changes indicate that plagioclase and Fe-Ti oxide fractionation is effective in the development of the pluton.
4. The crystallization temperatures calculated based on the apatite and zircon minerals vary between 739 and 872 °C.
4. All data indicate that the magma occurring the Artabel Pluton was generated by the partial melting of the meta-magmatic rocks.

Acknowledgements

This study was financially supported by Turkish Scientific Research Council (TÜBİTAK, Project No: 113Y382). We thank the editor and the anonymous reviewer for their improvement of the manuscript.

References

[1] Topuz, G., Altherr, R., Siebel, W., Schwarz, W.H., Zack, T., Hasözbek, A., Barth, M., Satır, M., Şen, C. Carboniferous high-potassium I-type granitoid magmatism in the Eastern Pontides: the Gümüşhane Pluton (NE Turkey). Lithos 2010; 116: 92–110.
[2] Dokuz, A. A Slab detachment and delamination model for the generation of Carboniferous high-potassium I-type magmatism in the Eastern Pontides, NE Turkey: Köse composite pluton. Gondwana Research 2011; 19: 926–944.
[3] Ustaömer, T., Robertson, A.H.F., Ustaömer, P.A., Gerdes, A., Peytcheva, I. Constraints on Variscan and Cimmerian magmatism and metamorphism in the Pontides (Yusufeli–Artvin area), NE Turkey from U–Pb dating and granite geochemistry: In: Robertson, A.H.F., Parlak, O., Ünlügenç, U.C., (eds.), Geological Development of Anatolia and the Easternmost Mediterranean Region. Geological Society of London Special Publications 2013; 372: 49–74.
[4] Kaygusuz, A., Arslan, M., Siebel, W., Sipahi, F., İlbeyli, N. Geochronological evidence and tectonic significance of Carboniferous magmatism in the southwest Trabzon area, eastern Pontides, Turkey. International Geology Rew 2012; 54 (15): 1776–1800.
[5] Kaygusuz, A., Arslan, M., Sipahi, F., Temizel, İ. U-Pb zircon chronology and petrogenesis of Carboniferous plutons in the northern part of the Eastern Pontides, NE Turkey: Constraints for Paleozoic magmatism and geodynamic evolution. Gondwana Research 2016; 39: 327–346.
[6] Dokuz, A. A slab Detachment and delamination model for the generation of Carboniferous high-potassium I-type magmatism in the Eastern Pontides, NE Turkey: Köse Composite Pluton. Godwana Research 2011; 19: 926-944.
[7] Karslı, O., Dokuz A, and Kandemir, R. Zircon Lu-Hf isotope systematics and U-Pb geochronology, whole-rock Sr-Nd isotopes and geochemistry of the early Jurassic Gökçedere pluton, Sakarya Zone-NE Turkey: a magmatic response to roll-back of the Paleo-Tethyan oceanic lithosphere. Contributions to Mineralogy and Petrology 2017; 172: 1–31.
[8] Yılmaz, S., Boztuğ, D. Space and time relations of three plutonic phases in the Eastern Pontides (Turkey). International Geology Review 1996; 38: 935–956.
[9] Karslı, O., Dokuz, A., Uysal, İ., Aydın, F., Chen, B., Kandemir, R., Wijbrans, J. Relative contributions of crust and mantle to generation of Campanian high-K calc-alkaline I-type granitoids in a subduction setting, with special reference to the Harşit Pluton (Eastern Turkey). Contributions to Mineralogy and Petrology 2010; 160: 467–487.
[10] Kaygusuz, A., Siebel, W., Şen, C., Satır, M. Petrochemistry and petrology of I-type granitoids in an arc setting: The composite Torul Pluton, Eastern Pontides (NE Turkey). International Journal of Earth Sciences 2008; 97: 739–764.
[11] Temizel, İ., Arslan, M., Yücel, C., Abdioğlu Yazar, E., Kaygusuz, A., Aslan, Z. U-Pb geochronology, bulk-rock geochemistry and petrology of Late Cretaceous syenitic plutons in the Gölköy (Ordu) area (NE Turkey): Implications for magma generation in a continental arc extension triggered by slab roll-back. Journal of Asian Earth Sciences 2019; 171: 305–320.
[12] Arslan, M., Aslan, Z. Mineralogy, petrography and whole-rock geochemistry of the Tertiary granitic intrusions in the Eastern Pontides (Turkey). Journal of Asian Earth Sciences 2006; 27: 177–193.
[13] Karslı, O., Chen, B., Aydın, F., Şen, C. Geochemical and Sr-Nd-Pb isotopic compositions of the Eocene Dölek and Sarıçiçek Plutons, Eastern Turkey: Implications for magma interaction in the genesis of high-K calc-alkaline granitoids in a post-collision extensional setting. Lithos 2007; 98: 67–96.
[14] Eyüboğlu, Y., Dudas, F.O., Thorkelson, D., Zhu, D.C., Liu, Z., Chatterjee, N., Yi, K., Santosh, M. Eocene granitoids of northern Turkey: Polybaric magmatism in an evolving arc–slab window system. Gondwana Research 2017; 50: 311–345.
[15] Temizel, İ., Abdioğlu Yazar, E., Arslan, M., Kaygusuz, A., Aslan, Z. Mineral chemistry, whole-rock geochemistry and petrology of Eocene I-type Shoshonitic plutons in the Gölköy area (Ordu, NE Turkey). Bulletin of the Mineral Research and Exploration 2018; 157: 121–152.
[16] Kaygusuz, A., Yücel, C., Arslan, M., Sipahi, F., Temizel, İ., Çakmak, G., Güloğlu, Z.S. Petrography, mineral chemistry and crystallization conditions of Tertiary plutonic rocks located to the north of Bayburt (Eastern

Pontides, Turkey). Bulletin of the Mineral Research and Exploration 2018; 157: 75–102.
[17] Kaygusuz, A., Yücel, C., Arslan, M., Temizel, İ., Yi, K., Jeong, Y-J., Siebel, W., Sipahi, F. Eocene I-type magmatism in the Eastern Pontides, NE Turkey: Insights into magma genesis and magma-tectonic evolution from whole-rock geochemistry, geochronology and isotope systematics. International Geology Review 2019; doi.org/10.1080/00206814.2019.1647468.
[18] Eyüboğlu, Y., Chung, S.L., Dudas, F.O., Santosh, M., Akaryalı, E. Transition from shoshonitic to adakitic magmatism in the Eastern Pontides, NE Turkey: Implications for slab window melting. Gondwana Research 2011; 19: 413–429.
[19] Saydam Eker, C., Sipahi, F., Kaygusuz A. Trace and rare earth elements as indicators of provenance and depositional environments of Liassic cherts in Gümüşhane, NE, Turkey. Chemie der Erde 2012; 72: 167–177.
[20] Aydınçakır, E. Subduction-related Late Cretaceous high-K volcanism in the Central Pontides orogenic belt: Constraints on geodynamic implications. Geodinamica Acta 2016; 28 (4): 379-411.
[21] Vural, A., Erdoğan, M. Eski Gümüşhane Kırkpavli alterasyon sahasında toprak jeokimyası çalışması, Gümüşhane, Türkiye. Güfbed/Gustij 2014; 4 (1): 1-15.
[22] Vural, A., Ersen, F. Geology, mineralogy and geochemistry of manganese mineralization in Gumushane, Turkey. Journal of Engineering Research and Applied Science 2019; 8: 1051–1059.
[23] Vural, A. K-Ar Dating for determining the age of mineralization as alteration product: A case study of antimony mineralization vein type in granitic rocks of Gümüşhane area, Turkey. Acta Physica Polonica A 2017; 132 (3): 792-795.
[24] Vural, A. Evaluation of soil geochemistry data of Canca area (Gümüşhane, Turkey) by means of inverse distance weighting (Idw) and kriging methods-preliminary findings. Bulletin of the Mineral Research and Exploration 2019; 158: 195-216.
[25] Kaygusuz, A., Şahin, K. Petrographical, geochemical and petrological characteristics of Eocene volcanic rocks in the Mescitli area, Eastern Pontides (NE Turkey). Journal of Engineering Research and Applied Science 2016; 5 (2): 473-486.
[26] Kaygusuz, A., Merdan Tutar, Z., Yücel, C. Mineral chemistry, crystallization conditions and petrography of Cenozoic volcanic rocks in the Bahçecik (Torul/Gümüşhane) area, Eastern Pontides (NE Turkey). Journal of Engineering Research and Applied Science 2017; 6 (2): 641–651.
[27] Sipahi, F., Akpınar, İ., Saydam Eker, Ç., Kaygusuz, A., Vural, A., Yılmaz, M. Formation of the Eğrikar (Gümüşhane) Fe–Cu skarn type mineralization in NE Turkey: U–Pb zircon age, litho-geochemistry, mineral chemistry, fluid inclusion, and O-H-C-S isotopic compositions. Journal of Geochemical Exploration 2017; 182: 32–52.
[28] Vural, A., Kaygusuz, A. Avliyana (Torul-Gümüşhane) Antimonit cevherleşmesinin jeolojisi-mineralojisi ve kökeninin araştırılması. Tübitak Projesi Sonuç Raporu 2016; Proje No: 113Y382.
[29] Yılmaz, Y. Petrology and structure of the Gümüşhane Granite and surrounding rocks, North-Eastern Anatolia. PhD Thesis 1972; University of London, 260 pp.
[30] Çoğulu, E. Gümüşhane ve Rize bölgelerinde petrolojik ve jeokronometrik araştırmalar. İ.T.Ü. Yayınları 1975, 1034, İstanbul, 112 p.
[31] Topuz, G., Altherr, R., Schwarz, W.H., Dokuz, A., Meyer, H.P. Variscan amphibolite-facies rocks from the Kurtoğlu metamorphic complex. Gümüşhane area, Eastern Pontides, Turkey. International Journal of Earth Sciences 2007; 96: 861-873.
[32] Eren, M. Gümüşhane-Kale arasının jeolojisi ve mikrofasiyes incelemesi. MMLS Tezi 1983; KÜ Fen Bilimleri Enstitüsü, Trabzon.
[33] Kandemir, R., Yılmaz, C. Lithostratigraphy, facies, and deposition environment of the Lower Jurassic Ammonitico Rosso type sedimentary (ARTS) in the Gümüşhane area, NE Turkey: Implications for the opening of the northern branch of the Neo-Tethys Ocean. Journal of Asian Earth Sciences 2009; 34: 586–598.
[34] Dokuz, A., Karslı, O., Chen, B., Uysal, İ. Sources and petrogenesis of Jurassic granitoids in the Yusufeli area, Northeastern Turkey: implications for pre- and post-collisional lithospheric thinning of the Eastern Pontides. Tectonophysics 2010; 480: 259–279.
[35] Boztuğ, D., Erçin, A.I., Kuruçelik, M.K., Göç, D., Kömür, I., İskenderoğlu, A. Geochemical characteristics of the Composite Kaçkar Batholith generated in A Neo-Tethyan convergence system, Eastern Pontides, Turkey. Joırnal of Asian Earth Sciences 2006; 27: 286-

302.
[36] Okay, A.I., Şahintürk, O. Geology of the Eastern Pontides, In: A. G. Robinson, (Ed.), Regional and petroleum geology of the Black Sea and surrounding region. AAPG Mem 1997; 68: 291-311.
[37] Topuz, G., Altherr, R., Schwarz, W.H., Siebel, W., Satır, M., Dokuz, A. Post-collisional plutonism with adakite-like signatures: the Eocene Saraycık Granodiorite (Eastern Pontides, Turkey). Contributions to Mineralogy and Petrology 2005; 150: 441–455.
[38] Karslı, O., Uysal, İ., Ketenci, M., Dokuz, A., Aydın, F., Chen, B., Kandemir, R., Wijbrans, J. Adakite-like granitoid porphyries in Eastern Pontides, NE Turkey: Potential parental melts and geodynamic implications. Lithos 2011; 127: 354-372.
[39] Eyüboğlu, Y., Santosh, M., Dudas, F,O., Akaryalı, E., Chung, S,L., Akdağ, K., Bektaş, O. The nature of transition from adakitic to non-adakitic magmatism in a slab-window setting: A synthesis from the Eastern Pontides, NE Turkey. Geoscience Frontiers 2013; 4: 353-375.
[40] Arslan, M., Temizel, İ., Abdioğlu, E., Kolaylı, H., Yücel, C., Boztuğ, D., Şen, C. 40Ar-39Ar dating, whole-rock and Sr-Nd-Pb isotope geochemistry of post-collisional Eocene volcanic rocks in the southern part of the Eastern Pontides (NE Turkey): Implications for magma evolution in extension-induced origin. Contributions to Mineralogy and Petrology 2013; 166: 113–142.
[41] Aydınçakır, E. The Petrogenesis of Early-Eocene non-adakitic volcanism in NE Turkey: Constraints on geodynamic implications. Lithos 2014; 208: 361–377.
[42] Arslan, M., Tüysüz, N., Korkmaz, S., Kurt, H. Geochemistry and petrogenesis of the eastern Pontide volcanic rocks, Northeast Turkey. Chemie der Erde 1997; 57: 157–187.
[43] Boztuğ, D., Jonckheere, R.C, Wagner, G.A., Yeğingil, Z. Slow Senonian and fast Paleocene-early Eocene uplift of the granitoids in the Central Eastern Pontides, Turkey: Apatite fission-track results. Tectonophysics 2004; 382 (3–4): 213–228.
[44] Temizel, İ., Arslan, M., Ruffet, G., Peucat, J.J. Petrochemistry, geochronology and Sr–Nd isotopic systematics of the Tertiary collisional and post-collisional volcanic rocks from the Ulubey (Ordu) area, Eastern Pontide, NE Turkey: implications for extension–related origin and mantle source characteristics. Lithos 2012; 128: 126–147.
[45] Yücel. C., Arslan, M., Temizel, İ., Abdioğlu, E. Volcanic facies and mineral chemistry of Tertiary volcanics in the northern part of the Eastern Pontides, northeast Turkey: implications for pre-eruptive crystallization conditions and magma chamber processes. Mineralogy and Petrology 2014; 108: 439–467.
[46] Korkmaz, S., Tüysüz, N., Er, M., Musaoğlu, A., Keskin, İ. Stratigraphy of Eastern Pontides, NE Turkey. In: Erler, A., et al. (Eds.), Geology of Black Sea Region Process of the International Symposium on the Geology of Black Sea Region. MTA, Ankara 1995: 59-66.
[47] Aydın, F., Karslı, O., Chen, B. Petrogenesis of the Neogene alkaline volcanics with implications for post–collisional lithospheric thinning of the Eastern Pontides, NE Turkey. Lithos 2008; 104: 249–266.
[48] Yücel, C., Arslan, M., Temizel, İ., Yazar, E.A., Ruffet, G. Evolution of K-rich magmas derived from a net veined lithospheric mantle in an ongoing extensional setting: Geochronology and geochemistry of Eocene and Miocene volcanic rocks from Eastern Pontides (Turkey). Gondwana Research 2017; 45: 65–86.
[49] Kaygusuz, A. K/Ar ages and geochemistry of the post-collisional volcanic rocks in the Ilıca (Erzurum) area, eastern Turkey. Neues Jahrbuch Für Mineralogie 2009; 186/1: 21-36.
[50] Kaygusuz, A., Aslan, Z., Aydınçakır, E., Yücel, C., Gücer, M.A., Şen, C. Geochemical and Sr-Nd-Pb isotope characteristics of the Miocene to Pliocene volcanic rocks from the Kandilli (Erzurum) area, Eastern Anatolia (Turkey): Implications for magma evolution in extension-related origin. Lithos 2018b; 296/299: 332-351.
[51] Streckeisen, A. To each plutonic rock its proper name, Earth Sciences Review 1976; 12: 1-33.
[52] Middlemost, E.A.K. Naming minerals in the magma/igneous rock system. Earth Sciences Review 1994; 37: 215–224.
[53] Le Maitre. R.W., Bateman, P., Dudek, A., Keller, J., Lameyre, J., Le Bas, M.J., Sabine, P.A., Schmid, R., Sorensen, H., Streckeisen, A., Woolley, A.R., Zanettin, B. A classification of igneous rocks and glossary of terms: Recommendations of the international union of geological sciences sub-commission on the systematics of igneous rocks. Blackwell

Scientific Publications 1989; Oxford, U.K. 193 pp.
[54] Sun, S.S., McDonough, W.F. Chemical and isotope systematics of oceanic basalts; Implication for Mantle Compositions and Processes. In. Saunders, A.D., and Nory, M.J., (eds.): Magmatism in the ocean basins. Geological Society of London, Special Publication 1989; 42: 313–345.
[55] Taylor, S.R., McLennan, S.M. The continental crust: Its composition and evolution. Blackwell Publication 1985; Oxford.
[56] Watson, E.B., Harrison, T.M. Zircon saturation revisited: Temperature and composition effects in a variety of crustal magma types. Earth Planet Sci Lett 1983; 64: 295–304
[57] Hanchar, J.M., Watson, E.B. Zircon saturation thermometry. In: Hanchar, J.M., Hoskin, P.W.O. (eds) Zircon. Rev in mineralogy and geochemistry. Mineralogical Society of America, Geochemical Society of America 2003; 53: 89–112
[58] Miller, C.F., McDowell, S.M., Mapes, R.W. Hot and cold granites? Implications of zircon saturation temperatures and preservation of inheritance. Geology 2003; 31: 529–532.
[59] Whalen, J.B., Currie, K.L., Chappell, B.W. A-type granites, chemical characteristics, discrimination and petrogenesis. Contributions to Mineralogy and Petrology 1987; 95: 407–419.
[60] Chappell, B.W., White, A.J.R. Two contrasting granite types. Pacific Geology 1974; 8: 173-204.
[61] Defant, M.J., Drummond, M.S. Derivation of some modern arc magmas by melting of young subducted lithosphere. Nature 1990; 347: 662–665.
[62] Pearce, J. A. Harris, N. B. W., Tindle, A.G. Trace elements discrimination diagram for the tectonic interpretation of granitic rock. Journal of Petrology 1984; 25/4: 43-63.
[63] Bacon, C.R., Druitt, T.H. Compositional evolution of the zoned calc-alkaline magma chamber of Mount Mazama, Crater Lake, Oregon. Contributions to Mineralogy and Petrology 1988; 98: 224–256.
[64] Grove, T.L., Donnelly-Nolan, J.M. The evolution of young silicic lavas at Medicine Lake Volcano, California: Implications for the origin of compositional gaps in calc-alkaline series lavas. Contribution to Mineralogy and Petrology 1986; 92: 281–302.
[65] Roberts, M.P., Clemens, J.D. Origin of high-potassium, calc-alkaline, I-type granitoids. Geology 1993; 21: 825–828.
[66] Guffanti, M., Clynne, M.A., Muffler, L.J.P. Thermal and mass implications of magmatic evolution in the Lassen Volcanic Region, California, and minimum constraints on basalt influx to the lower crust. Journal of Geophysical Research 1996; 101: 3001–3013.
[67] Rapp, R.P., Watson, E.B. Dehydration melting of metabasalt at 8–32 kbar: Implications for continental growth and crust-mantle recycling. Journal of Petrology 1995; 36: 891–931.
[68] Patino Douce, A.E., Beard, J.S. Effects of P, f (O2) and Mg/Fe ratio on dehydration melting of model metagreywackes. Journal of Petrology; 37: 999–1024.
[69] Patiño Douce, A.E. What do experiments tell us about the relative contributions of crust and mantle to the origin of granitic magmas? In: Castro, A., Fernandez, C., Vigneresse, J.L. (Eds.), Understanding granites: Integrating new and classical techniques. Geological Society, London, Special Publications 1999; 168: 55–75.